PROCEEDINGS OF SCIENCE

NLO QCD corrections to $Wb\bar{b}$ and $Zb\bar{b}$ production

Fernando Febres Cordero
University of California, Los Angeles
E-mail: ffebres@physics.ucla.edu

Laura Reina[*]
Florida State University
E-mail: reina@hep.fsu.edu

Doreen Wackeroth
University at Buffalo - The State University of New York
E-mail: dow@ubpheno.physics.buffalo.edu

We present NLO QCD results for $Wb\bar{b}$ and $Zb\bar{b}$ production at the Tevatron including full bottom-quark mass effects. We study the impact of QCD corrections on both total cross-section and invariant mass distribution of the bottom-quark pair. Including NLO QCD corrections greatly reduces the dependence of the tree-level cross-section on the renormalization and factorization scales. We also compare our calculation to a calculation that considers massless bottom quarks and find that the bottom-quark mass effects amount to about 8-10% of the total NLO QCD cross-section and can impact the shape of the bottom-quark pair invariant mass distribution, in particular in the low invariant mass region.

8th International Symposium on Radiative Corrections
October 1-5, 2007
Florence, Italy

[*]Speaker.

1. Introduction

Precise theoretical predictions for the production of a weak gauge boson (W/Z) in association with a $b\bar{b}$ pair are very important both in the search for a light Standard Model (SM)-like Higgs boson and in the search for single-top production at hadron colliders, in particular at the Tevatron. Indeed, $W/Z+b\bar{b}$ represent the major irreducible backgrounds to the associated production of a light Higgs boson with a weak gauge boson (WH and ZH with $H\to b\bar{b}$), which are the main search modes for a SM-like Higgs boson at the Tevatron [1, 2]. At the same time, $Wb\bar{b}$ is an irreducible background for single-top production, which is being measured for the first time at the Tevatron as $p\bar{p}\to t\bar{b},\bar{t}b$ with $t(\bar{t})\to b(\bar{b})W$ [3, 4].

The signal cross sections for both WH/ZH and single-top production are known including higher order QCD and electroweak corrections. It is therefore important to also control the background to a good level of theoretical precision. In the present experimental analyses the effects of Next-to-Leading (NLO) QCD corrections on the total cross-section and the dijet invariant mass distribution of the $Wb\bar{b}$ and $Zb\bar{b}$ background processes have been taken into account by using the MCFM package [5], which implements the zero bottom-quark mass ($m_b=0$) approximation [6, 7, 8].

In this proceedings we present results for the NLO QCD cross-sections and $b\bar{b}$-pair invariant mass distributions at the Tevatron, including full bottom-quark mass effects [9]. We separately study the impact of NLO QCD corrections and of non-zero bottom-quark mass effects. NLO QCD corrections stabilize the theoretical prediction of total cross-sections and distributions, reducing the dependence on the renormalization and factorization scales. On the other hand, the presence of a non-zero bottom-quark mass mainly affect the cross-section in the region where the $b\bar{b}$-pair invariant mass is small, both at Leading Order (LO) and at NLO in QCD, and amount to an overall 8-10% difference with respect to the zero bottom-quark mass approximation.

2. NLO calculation

The hadronic production of a W boson with a $b\bar{b}$ pair occurs at tree level in QCD via the $q\bar{q}'\to Wb\bar{b}$ partonic process. On the other hand, the hadronic production of a Z boson with a $b\bar{b}$ pair consists, at the tree level in QCD, of two partonic channels, namely $q\bar{q}\to Zb\bar{b}$ and $gg\to Zb\bar{b}$. The NLO QCD corrections to the tree level partonic cross-section consists of both one-loop $O(\alpha_s)$ virtual corrections and $O(\alpha_s)$ real corrections corresponding to the emission of one extra parton from the tree level parton processes. The NLO hadronic cross-section is obtained by convoluting the parton-level NLO cross-sections with NLO Parton Distribution Functions (PDF).

The $O(\alpha_s)$ virtual corrections to the partonic cross-section contain ultraviolet (UV) and infrared (IR) singularities. The UV singularities are calculated using dimensional regularization and cancelled by introducing a suitable set of counterterms (see Ref. [9] for details). IR singularities are isolated using dimensional regularization and cancelled against the analogous singularities arising in the $O(\alpha_s)$ real corrections to the partonic cross-section.

The $O(\alpha_s)$ virtual corrections to the partonic cross-section consist of one-loop self-energy, vertex, box and pentagon diagrams. We apply techniques developed in the NLO QCD calculation of $Ht\bar{t}$ [10, 11] for the calculation of scalar and tensor loop-integrals. In particular, we calculate

the tensor loop-integrals via Passarino-Veltman reduction (PV) [12]. We encounter instabilities due to the quasi-vanishing of the Gram determinant(s) of the process only in one box diagram and in several pentagon diagrams. We are able to obtain stable numerical results by combining, when necessary, sets of gauge invariant diagrams.

The $O(\alpha_s)$ real corrections to the partonic cross-section consist of the $q\bar{q}' \to Wb\bar{b}+g$ and $qg(\bar{q}g) \to Wb\bar{b}+q(\bar{q})$ subprocesses for $Wb\bar{b}$ production and of the $q\bar{q} \to Zb\bar{b}+g$, $gg \to Zb\bar{b}+g$, and $qg(\bar{q}g) \to Zb\bar{b}+q(\bar{q})$ subprocesses for $Zb\bar{b}$ production. We have extracted both soft and collinear IR singularities by implementing a Phase Space Slicing method with two cutoffs [13] in order to isolate the soft (δ_s) and collinear (δ_c) singularities respectively. Both the soft, hard-collinear, and hard-non-collinear parts of the cross-section depend on the cutoffs, but their sum is cutoff independent over a large range of values of the cutoffs (see Ref. [9]).

Both analytical and numerical results for the NLO hadronic cross-section have been checked with two independent calculations based on different programming languages and public/in-house packages. The analytical reduction of the calculation has been obtained using FORM [14] and *Maple* codes, while the numerical results have been obtained using Fortran and C codes. The FF package [15] has been used to check some of the IR-finite scalar and tensor integrals. Finally, the hard non-collinear real corrections have been double-checked using Madgraph [16, 17, 18].

3. Numerical results

In these proceedings we present results for $Wb\bar{b}$ and $Zb\bar{b}$ production at the Tevatron including NLO QCD corrections and a non-zero bottom-quark mass fixed at $m_b = 4.62$ GeV. Results for $Wb\bar{b}$ have been published in Ref. [9], while results for $Zb\bar{b}$ are currently being cross-checked and should be considered as preliminary. Both W and Z boson are considered on-shell and their masses are taken to be $M_W = 80.41$ GeV for the $Wb\bar{b}$ runs and $M_Z = 91.1876$ GeV for the $Zb\bar{b}$ runs, while, in each case, the other weak gauge boson mass is calculated via the relation $M_W = \cos\theta_w M_Z$ with $\sin^2\theta_w = 0.223$. The LO results use the 1-loop evolution of α_s and the CTEQ6L set of PDF [19], while the NLO results use the 2-loop evolution of α_s and the CTEQ6M set of PDF, with $\alpha_s^{NLO}(M_Z) = 0.118$. The W boson coupling to quarks is proportional to the Cabibbo-Kobayashi-Maskawa (CKM) matrix elements. We take $V_{ud} = V_{cs} = 0.975$ and $V_{us} = V_{cd} = 0.222$, while we neglect the contribution of the third generation, since it is suppressed either by the initial state quark densities or by the corresponding CKM matrix elements.

We implement the k_T jet algorithm [20, 21, 22, 23] with a pseudo-cone size $R = 0.7$ and we recombine the parton momenta within a jet using the so called covariant E-scheme [21]. We checked that our implementation of the k_T jet algorithm coincides with the one in MCFM. We require all events to have a $b\bar{b}$ jet pair in the final state, with a transverse momentum larger than 15 GeV ($p_T^{b,\bar{b}} > 15$ GeV) and a pseudorapidity that satisfies $|\eta^{b,\bar{b}}| < 2$. We impose the same p_T and $|\eta|$ cuts also on the extra jet that may arise due to hard non-collinear real emission of a parton, i.e. in the processes $W/Zb\bar{b}+g$ or $W/Zb\bar{b}+q(\bar{q})$. This hard non-collinear extra parton is treated either *inclusively* or *exclusively*, following the definition of *inclusive* and *exclusive* as implemented in the MCFM code [5]. In the *inclusive* case we include both two- and three-jet events, while in the *exclusive* case we require exactly two jets in the event. Two-jet events consist of a bottom-quark jet pair that may also include a final-state light parton (gluon or quark) due to the applied

recombination procedure. Results in the massless bottom-quark approximation have been obtained using the MCFM code [5].

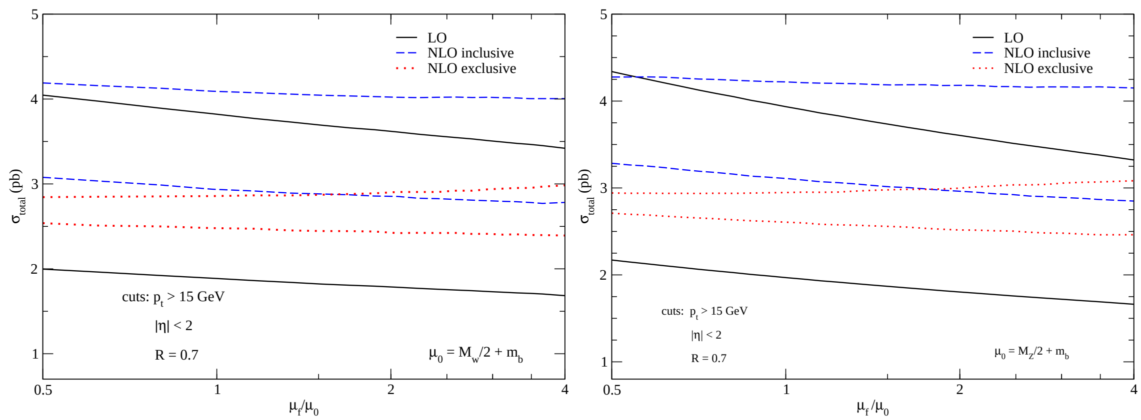

Figure 1: Dependence of the LO (black solid band), NLO *inclusive* (blue dashed band), and NLO *exclusive* (red dotted band) total cross-sections on the renormalization/factorization scales, including full bottom-quark mass effects. The l.h.s. plot is for $p\bar{p} \to Wb\bar{b}$ and the r.h.s. plot for $p\bar{p} \to Zb\bar{b}$. The bands are obtained by varying both μ_R and μ_F independently between $\mu_0/2$ and $4\mu_0$ (with $\mu_0 = m_b + M_V/2$ for $V = W,Z$ in the $p\bar{p} \to Wb\bar{b}$ and $p\bar{p} \to Zb\bar{b}$ cases respectively).

In Fig. 1 we illustrate the renormalization and factorization scale dependence of the LO and NLO total cross-sections, both in the *inclusive* and *exclusive* case. The bands are obtained by varying both μ_R and μ_F independently between $\mu_0/2$ and $4\mu_0$ (with $\mu_0 = m_b + M_V/2$ for $V = W,Z$ in the $p\bar{p} \to Wb\bar{b}$ and $p\bar{p} \to Zb\bar{b}$ cases respectively), including full bottom-quark mass effects. We notice that the NLO cross-sections have a reduced scale dependence over most of the range of scales shown, and the *exclusive* NLO cross-section is more stable than the *inclusive* one especially at low scales. While the LO cross-section still has a 40% uncertainty due to scale dependence, this uncertainty is reduced at NLO to about 20% for the *inclusive* and to about 10% for the *exclusive* cross-section respectively. This is consistent with the fact that the *inclusive* NLO cross-section integrates over the entire phase space of the $qg(\bar{q}g) \to b\bar{b}W/Z + q(\bar{q})$ channels that are evaluated with NLO α_s and NLO PDF, but are actually tree-level processes and retain therefore a strong scale dependence. In the *exclusive* case only the $2 \to 3$ collinear kinematic of these processes is retained, since 3-jets events are discarded, and this makes the overall renormalization and factorization scale dependence milder. This is better illustrated in Fig. 2 for the case of $p\bar{p} \to Zb\bar{b}$, where the r.h.s. plots show the scale dependence of the cross-sections due to the single partonic channels ($q\bar{q}$, gg and $qg + \bar{q}g$). The strong residual scale dependence of the *inclusive* NLO cross-section is clearly driven by the $qg + \bar{q}g$ channel. Similar results are obtained for $p\bar{p} \to Wb\bar{b}$, as reported in Ref. [9].

A first illustration of the impact of keeping a non-zero bottom-quark mass in the calculation of the NLO QCD cross-section is given in the l.h.s. plots of Fig. 2, where LO and NLO total cross-sections for $p\bar{p} \to Zb\bar{b}$ are given, both for $m_b = 0$ and $m_b = 4.62$ GeV, as functions of the renormalization and factorization scales (identified for the purpose of this plot). Neglecting bottom-quark mass effects overestimate the NLO cross-section by about 8-10%, depending on the choice of the scale. In Fig. 3 we analyze the impact of a non-zero bottom-quark mass on the $b\bar{b}$-pair

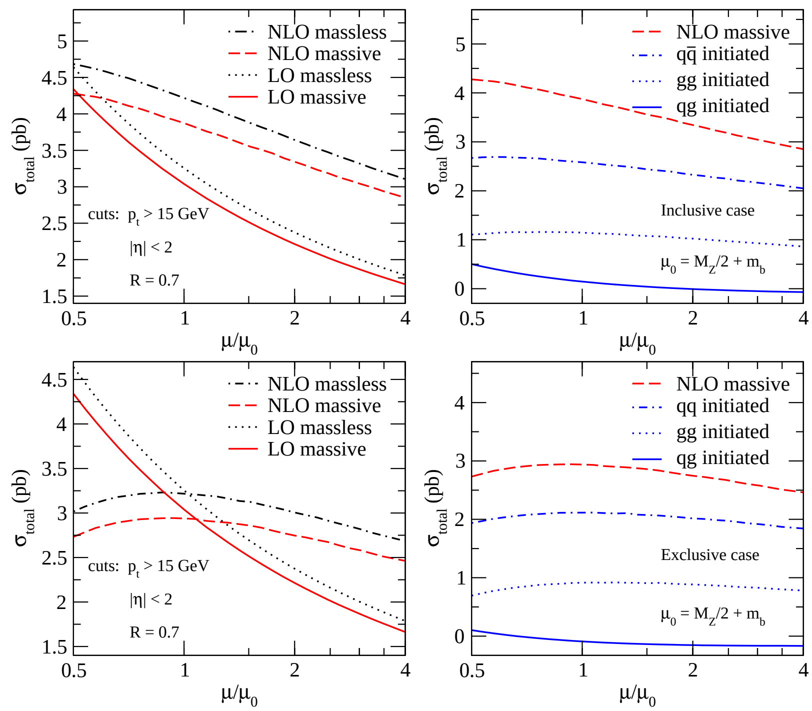

Figure 2: Dependence of the LO and NLO *inclusive* (upper plots) and *exclusive* (lower plots) total cross-section for $p\bar{p} \to Zb\bar{b}$ on the renormalization/factorization scale, when $\mu_R = \mu_F$. The l.h.s. plots compare both LO and NLO total cross-sections for the case in which the bottom quark is treated as massless (MCFM) or massive (our calculation). The r.h.s. plots show separately, for the massive case only, the scale dependence of the $q\bar{q}$, gg and $qg + \bar{q}g$ contributions, as well as their sum.

invariant-mass ($m_{b\bar{b}}$) distribution. We give results for both *inclusive* and *exclusive* distribution in the $p\bar{p} \to Wb\bar{b}$ case. In both cases distributions most of the impact is in the low $m_{b\bar{b}}$ region, which can be important in a variety of different analyses.

References

[1] V. M. Abazov *et al.*, the D0 Collaboration [arXiv:0712.0598v1].

[2] A. Abulencia *et al.*, the CDF Collaboration, *Phys. Rev. Lett.* **96** (2006) 081803.

[3] V. M. Abazov *et al.*, the D0 Collaboration *Phys. Rev. Lett.* **99** (2007) 191802 [hep-ex/0702005v1].

[4] D. Acosta *et al.*, the CDF Collaboration, *Phys. Rev. D* **71** (2005) 012005, [hep-ex/0410058].

[5] J. Campbell and R. K. Ellis, *MCFM - A Monte Carlo for FeMtobarn processes at Hadron Colliders*, available at [http://mcfm.fnal.gov].

[6] R. K. Ellis and S. Veseli, *Phys. Rev. D* **60** (1999) 011501(R), [hep-ph/9810489].

[7] J. Campbell and R. K. Ellis, *Phys. Rev. D* **62** (2000) 114012, [hep-ph/0006304].

[8] J. Campbell and R. K. Ellis, *Phys. Rev. D* **65** (2002) 113007, [hep-ph/0202176].

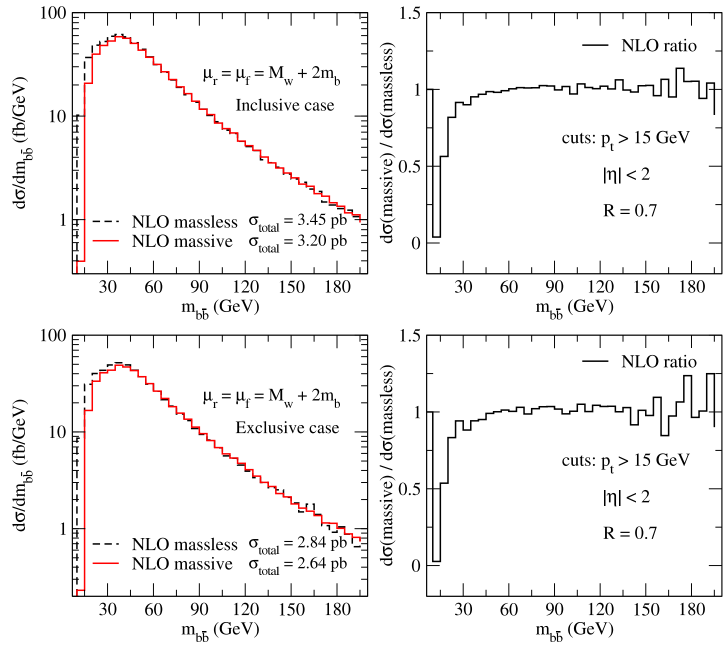

Figure 3: The *inclusive* (upper plots) and *exclusive* (lower plots) distributions, $d\sigma/dm_{b\bar{b}}$, for $p\bar{p} \to Wb\bar{b}$ derived from our calculation (with $m_b \neq 0$) and from MCFM (with $m_b = 0$). The right hand side plot shows the ratio of the two distributions, $d\sigma(m_b \neq 0)/d\sigma(m_b = 0)$. From Ref. [9].

[9] F. Febres Cordero, L. Reina and D. Wackeroth, *Phys. Rev. D* **74** (2006) 034007, [`arXiv:hep-ph/0606102`].

[10] L. Reina, S. Dawson, and D. Wackeroth, *Phys. Rev. D* **65** (2002) 053017, [`hep-ph/0109066`].

[11] S. Dawson, C. Jackson, L. H. Orr, L. Reina, and D. Wackeroth, *Phys. Rev. D* **68** (2003) 034022, [`hep-ph/0305087`].

[12] G. Passarino and M. J. G. Veltman, *Phys. Lett. B* **237** (1990) 537.

[13] B. W. Harris and J. F. Owens, *Phys. Rev. D* **65** (2002) 094032", [`hep-ph/0102128`].

[14] J. A. M. Vermaseren, "*New features of FORM*" (2000) [`math-ph/0010025`].

[15] G. J. van Oldenborgh, *Comput. Phys. Commun.* **66** (1991) 1-15.

[16] H. Murayama, I. Watanabe, and K. Hagiwara, " *HELAS: HELicity amplitude subroutines for Feynman diagram evaluations*" (1992), KEK-91-11.

[17] T. Stelzer and W. F. Long, *Comput. Phys. Commun.* **81** (1994) 357, [`hep-ph/9401258`].

[18] F. Maltoni and T. Stelzer, *JHEP* **02** (2003) 27, [`hep-ph/0208156`].

[19] H. L. Lai and others, *the CTEQ collaboration*, *Eur. Phys. J. C* **12** (2000) 375, [`hep-ph/9903282`].

[20] S. Catani, Y. L. Dokshitzer, and B. R. Webber, *Phys. Lett. B* **285** (1992) 291.

[21] S. Catani, Y. L. Dokshitzer, M. H. Seymour, and B. R. Webber, *Nucl. Phys. B* **406** (1993) 187.

[22] S. D. Ellis and D. E. Soper, *Phys. Rev. D* **48** (1993) 3160, [`hep-ph/9305266`].

[23] W. B. Kilgore and W. T. Giele, *Phys. Rev. D* **55** (1997) 7183, [`hep-ph/9610433`].